A Comprehensive Model for the Allosteric Regulation of Mammalian Ribonucleotide Reductase. Functional Consequences of ATP- and dATP-Induced Oligomerization of the Large Subunit†

Ossama B. Kashlan,‡,§ Charles P. Scott,‡,§,|| James D. Lear,⊥ and Barry S. Cooperman*,‡

Department of Chemistry, University of Pennsylvania, Philadelphia, Pennsylvania 19104-6323, and Department of Biochemistry and Biophysics, School of Medicine, University of Pennsylvania, Philadelphia, Pennsylvania 19104

Received August 13, 2001; Revised Manuscript Received October 25, 2001

ABSTRACT: Reduction of NDPs by murine ribonucleotide reductase (mRR) requires catalytic (mR1) and free radical-containing (mR2) subunits and is regulated by nucleoside triphosphate allosteric effectors. Here we present a new, comprehensive, and quantitative model for allosteric control of mRR enzymatic activity based on molecular mass, ligand binding, and enzyme activity studies. In this model, nucleotide binding to the specificity site (s-site) drives formation of an active $R1_2R2_2$ dimer, ATP or dATP binding to the adenine-specific site (a-site) results in formation of an inactive tetramer, and ATP binding to the newly described hexamerization site (h-site) drives formation of active $R1_6R2_6$ hexamer. In contrast, an earlier phenomenological model [Thelander, L., and Reichard, P. (1979) *Annu. Rev. Biochem. 67*, 71−98] (the "RT" model) ignores aggregation state changes and mistakenly rationalizes ATP activation versus dATP inhibition as reflecting different functional consequences of ATP versus dATP binding to the a-site. Our results suggest that the $R1_6R2_6$ heterohexamer is the major active form of the enzyme in mammalian cells, and that the ATP concentration is the primary modulator of enzyme activity, coupling the rate of DNA biosynthesis with the energetic state of the cell. Using the crystal structure of the *Escherichia coli* R1 hexamer as a model for the mR1 hexamer, a scheme is presented that rationalizes the slow isomerization of the tetramer form and suggests an explanation for the low enzymatic activity of tetramers complexed with R2. The similar specific activities of $R1_2R2_2$ and $R1_6R2_6$ are inconsistent with a proposed model for $R2_2$ docking with $R1_2$ [Uhlin, U., and Eklund, H. (1994) *Nature 370*, 533−539], and an alternative is suggested.

Ribonucleotide reductases (RRs)[1] form a family of allosterically regulated enzymes that catalyze the conversion of ribonucleotides to 2′-deoxyribonucleotides (*1*), providing the deoxynucleotide substrates that are essential for de novo DNA biosynthesis. Class Ia RRs, which comprise all eukaryotic RRs as well as some from eubacteria, bacteriophages, and viruses (*1*), accept the four common nucleoside diphosphates (NDPs) as substrates, with enzymatic activity that is dependent upon the formation of a complex between two different subunits, R1 and R2. The R2 subunit contains a stable tyrosyl free radical that is necessary for NDP reduction (*2*). The enzymatic active site, and all sites for allosteric ligands, are located on the R1 subunit.

In the well-accepted phenomenological model of Reichard and Thelander (refs *1*, *3*, and *4*, the "RT" model), binding of effectors to two classes of sites accounts for allosteric regulation of ribonucleotide reductase. Binding to the specificity site (s-site) dictates substrate selection, while global enzymatic activity is determined by ligand binding to the activity site (a-site). The RT model rationalizes binding and activity data for several class Ia RRs, providing a valuable qualitative guide for predicting which activity will be manifest under specific conditions. According to this model, ATP and dATP can bind to both allosteric sites while dTTP and dGTP bind to only the s-site (*5*, *6*). The reduction of specific NDPs by RR varies according to the occupancy of these sites. ATP stimulates the reduction of CDP and UDP (*7*), and dTTP stimulates the reduction of GDP; dGTP stimulates the reduction of ADP, and dATP serves as a general inhibitor (*8*−*10*). This elaborate regulatory scheme ensures a balanced pool of deoxynucleotide monomers for DNA replication.

Although the RT model gives a succinct accounting of the phenomenology of regulation, it provides little insight into the molecular mechanism by which regulation is achieved. The goal of our research over the last several years has been to develop a quantitative mechanistic model for

† Supported by NIH Grants CA58567 (to B.S.C.) and GM07229 (to C.P.S.).

* To whom correspondence should be addressed. Telephone: (215) 898-6330. Fax: (215) 898-2037. E-mail: cooprman@pobox.upenn.edu.

‡ Department of Chemistry.

§ These authors contributed equally to this work.

|| Current address: Structural Biology and Bioinformatics Program, Kimmel Cancer Center, Thomas Jefferson University, 833 Bluemle Life Sciences Building, 233 S. 10th St., Philadelphia, PA 19107.

⊥ Department of Biochemistry and Biophysics, School of Medicine.

[1] Abbreviations: DLS, dynamic light scattering; MALLS, multiangle laser light scattering; mRR, murine ribonucleotide reductase; mR1, murine ribonucleotide reductase large subunit; mR2, murine ribonucleotide reductase small subunit; NDPs, nucleoside diphosphates; RR, ribonucleotide reductase; RT model, Reichard−Thelander model; R1, ribonucleotide reductase large subunit; R2, ribonucleotide reductase small subunit; SE, sedimentation equilibrium; SV, sedimentation velocity.

10.1021/bi011653a CCC: $22.00
Published on Web 12/14/2001

Scheme 1: ATP and dATP Effects on Enzyme Aggregation State and Activity[a]

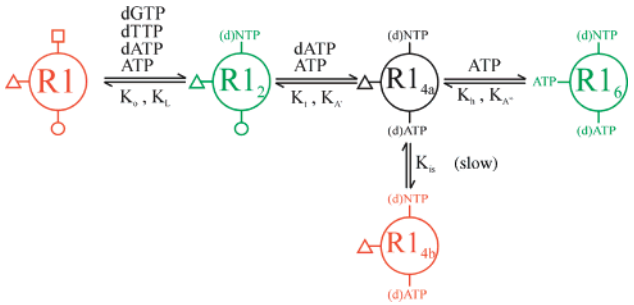

[a] R2 has been omitted for simplicity; activity assays were carried out in the presence of a saturating R2 concentration. States shown in green have high activity, and those in red have little or no activity. The activity of $R1_{4a}$ is not known (see the text). □, ○, and △ represent the s-, a-, and h-sites, respectively.

the regulation of RR. In previous work (*15*), we focused on the mechanism by which specificity toward purine diphosphates is engendered, and developed a quantitative 16-state model for s-site-mediated activation. In this model, both the substrate and effector promote mR1 dimerization, giving rise to apparent heterotropic cooperativity. When these effects on dimerization are taken into account, specificity in substrate reduction is seen to result primarily from effects on k_{cat} (an allosteric V-system) rather than from effects on K_m (an allosteric K-system). This result underlines the importance of quaternary structure for the allosteric regulation of mRR, something which the RT model totally ignores.

Here we extend our scope by formulating the more general model, shown in Scheme 1, that accounts quantitatively for the modulation of RR enzymatic activity toward all four NDP substrates by ATP and dATP, and further demonstrates the centrality of ligand-dependent changes in R1 quaternary structure for mRR regulation. In formulating this model, we were cognizant of earlier studies showing that both ATP and dATP promote the formation of high-molecular weight R1 species (*9*, *11*−*13*). The main features of Scheme 1, which is based on the molecular weight, ligand binding, and activity studies presented below, are as follows: (1) ATP or dATP binding to the s- and a-sites drives formation of $R1_2$ and $R1_4$, respectively; (2) $R1_4$ exists in two, slowly equilibrating, conformations, $R1_{4a}$ and $R1_{4b}$, with the latter predominating at equilibrium; (3) ATP binding to a newly described h-site drives formation of $R1_6$; and (4) the $R2_2$ complexes of both $R1_2$ and $R1_6$ are enzymatically active, whereas the $R2_2$ complex $R1_{4b}$ has little activity.

Our results make it clear that the properties attributed in the RT model to the "activity site" mistakenly conflate the properties of two sites: one that binds both ATP and dATP and promotes the formation of an R1 tetramer with low enzymatic activity toward all four NDP substrates, and the h-site. We rename the former as the "adenine site", which, abbreviated as the "a-site", maintains an apparent consistency within the literature.

EXPERIMENTAL PROCEDURES

Materials

Recombinant mR1 and mR2 were prepared as described previously (*15*). [^{3}H]dATP was purchased from ICN Radiochemicals (Irvine, CA). All other materials were of the highest available purity.

Methods

The following methods were carried out at 25 °C, except as otherwise indicated, as described previously (*15*): determinations of protein and nucleotide concentrations and of nucleotide purity; measurements and analyses of dynamic light scattering (DLS), sedimentation velocity (SV), and sedimentation equilibrium (SE); and assays of dATP binding and enzyme activity. For the latter, all components of the reaction mixture were preincubated for 7 min prior to substrate addition except as otherwise indicated. All enzyme activity data are reported as the average of duplicate measurements ± the average deviation, unless otherwise indicated. DLS experiments were carried out at 22 ± 3 °C. All DLS data are reported as averages ± the standard deviation (≥10 determinations per point). R1 and R2 concentrations are reported as monomer, unless otherwise indicated.

Multiangle Laser Light Scattering (MALLS). MALLS studies were carried out at 22 ± 3 °C using a DAWN DSP laser photometer from Wyatt Technologies (Santa Barbara, CA) (*16*). The instrument was used in the microbatch mode, with samples being introduced into the flow cell via a 0.1 μm filter using a syringe pump. Maximum stable scattering, collected at all 17 angles, was achieved within 2 min of sample preparation. Scattering data were analyzed using the ASTRA software (Wyatt Technologies) that was supplied with the instrument. Relative weight-averaged molecular masses were determined by extrapolation of Debye plots of $R(\theta)/K^*c$ versus $\sin^2(\theta/2)$ to zero angle, where θ is the scattering angle, $R(\theta)$ is the excess intensity (I) of scattered light at that angle, c is the concentration of the sample, and K^* is a constant equal to $4\pi^2n^2(dn/dc)^2/\lambda_0^4N_A$ (n is the solvent refractive index, dn/dc is the refractive index increment of the scattering sample, λ_0 is the wavelength of scattered light, and N_A is Avogadro's number) (*16*).

Buffers

MALLS and DLS Experiments. Buffer B was 50 mM (hydroxyethyl)piperazineethanesulfonic acid (HEPES) (pH 7.6), 25 mM DTT, 10 mM KCl, 10 mM $MgCl_2$, and 7 mM NaF.

SV and SE Experiments. Buffer C was 50 mM Tris-HCl (pH 7.6), 10 mM KCl, 10 mM $MgCl_2$, 25 mM β-mercaptoethanol, and 7 mM NaF. $FeCl_3$ (50 μM) was added to the buffer in samples containing R2.

In dNTP binding and enzymatic activity experiments, buffer B was supplemented with 50 μM $FeCl_3$.

Equations for Curve Fitting

Equations used for curve fitting are presented in Tables 1 (equilibrium constants and conservation, eqs 1−11) and 2 (measurements, eqs 12−17).

Equilibria and Conservation

Equilibrium Constants. Seven equilibrium constants define the relationships between the various species in Scheme 1 (eqs 1−7). In these equations, L refers to dTTP, dGTP,

Table 1: Equations for Equilibrium Constants and Conservation

equilibrium constants

$$K_L = (2[R1_2][L])/[R1_2L] = (0.5[R1_2L][L])/[R1_2L_2] \quad (1)$$

$$K_{A'} = (4[R1_{4a}L_i][A])/[R1_{4a}L_iA'] = (0.25[R1_{4a}L_iA'_3][A])/[R1_{4a}L_iA'_4], \text{ where } i = 0-4 \quad (2)$$

$$K_{A''} = (6[R1_6L_iA'_j][A])/[R1_6L_iA'_jA''] = ({}^1/_6[R1_6L_iA'_jA''_5][A])/[R1_6L_iA'_jA''_6], \text{ where } i \text{ and } j = 0-6 \quad (3)$$

$$K_o = [R1]^2/[R1_2] \quad (4)$$

$$K_t = [R1_2]^2/[R1_{4a}] = [R1_2L_2]^2/[R1_{4a}L_4] \quad (5)$$

$$K_h = ([R1_2][R1_{4a}])/[R1_6] \quad (6)$$

$$K_{is} = [R1_{4b}]/[R1_{4a}] \quad (7)$$

definitions

$\alpha = [L]/K_L$; $\beta = [A]/K_{A'}$; $\gamma = [A]/K_{A''}$; α_c, β_c, and γ_c are defined equivalently for a competitive ligand

conservation of R1with varying [ATP] or [dATP]

in the absence of a competing ligand

$$[R1]_T = [R1]_t + 2[R1_2]_t + 4[R1_4]_t + 6[R1_6]_t \quad (8a)$$

$$[R1]_t = [R1] \quad (8b)$$

$$[R1_2]_t = \sum_{i=0}^{2}[R1_2L_i] = [R1_2](1+\alpha)^2 \quad (8c)$$

$$[R1_4]_t = [R1_{4a}]_t + [R1_{4b}]_t = \sum_{i=0}^{4}\sum_{j=0}^{4}[R1_{4a}L_iA'_j] + \sum_{i=0}^{4}\sum_{j=0}^{4}[R1_{4b}L_iA'_j] = [R1_{4a}](1+K_{is})(1+\alpha)^4(1+\beta)^4 \quad (8d)$$

$$[R1_6]_t = \sum_{i=0}^{6}\sum_{j=0}^{6}\sum_{k=0}^{6}[R1_6L_iA'_jA''_k] = [R1_6](1+\alpha)^6(1+\beta)^6(1+\gamma)^6 \quad (8e)$$

in the presence of dTTP or dGTP

$$[R1]_T = [R1] + [R1_2](1+\alpha+\alpha_c)^2 + [R1_{4a}](1+K_{is})(1+\alpha+\alpha_c)^4(1+\beta)^4 + [R1_6](1+\alpha+\alpha_c)^6(1+\beta)^6(1+\gamma)^6 \quad (9a)$$

in the presence of a saturating [dTTP] or [dGTP]

$$[R1]_T = 2\left[[R1_2L_2] + \frac{[R1_2L_2]^2}{K_t}(1+K_{is})(1+\beta)^4 + \frac{[R1_2L_2]^3}{K_tK_h}(1+\beta)^6(1+\gamma)^6\right] \quad (9b)$$

in the presence of a competing ligand for s-, a-, and h-sites

$$[R1]_T = [R1] + [R1_2](1+\alpha+\alpha_c)^2 + [R1_{4a}](1+K_{is})(1+\alpha+\alpha_c)^4(1+\beta+\beta_c)^4 + [R1_6](1+\alpha+\alpha_c)^6(1+\beta+\beta_c)^6(1+\gamma+\gamma_c)^6 \quad (10)$$

conservation of dATP

$$[A]_T = [A] + \sum_{i=0}^{2} i[R1_2L_i] + \sum_{i=0}^{4}\sum_{j=0}^{4}(i+j)[R1_{4a}L_iA'_j](1+K_{is}) + \sum_{i=0}^{6}\sum_{j=0}^{6}\sum_{k=0}^{6}(i+j+k)[R1_6L_iA'_jA''_k] \quad (11)$$

dATP, or ATP and A refers to ATP or dATP. There are three different allosteric sites. Ligands occupying the s-, a-, and h-sites site are unprimed (L), primed (A′), and double-primed (A″), respectively. The dissociation constants K_L, $K_{A'}$, and $K_{A''}$ describe ligand affinity, with the following assumptions: (1) s-site binding occurs to the dimer, both tetramers, and the hexamer with the same dissociation constant K_L; (2) a-site binding occurs to both tetramers and the hexamer with the same dissociation constant $K_{A'}$; (3) h-site binding occurs only to the hexamer with the dissociation constant $K_{A''}$. Allowing a-site binding to dimers and h-site binding to both dimers and tetramers gave values for dissociation constants that were extremely high, so such binding can be safely ignored. Three other constants (K_o, K_t, and K_h) describe R1 oligomerization. Finally, K_{is} defines tetramer isomerization.

R1 Conservation. For ATP and dATP titrations, $[R1]_T$ is given by four equations, depending on the circumstances of the experiment. Equations 8a−e apply when ATP or dATP is added alone; eqs 9a and 9b apply in the presence of dGTP or dTTP, and of saturating dGTP or dTTP, respectively, and eq 10 applies when ATP and dATP are both present.

Nucleotide Conservation. Except for dATP, measurements were always taken at nucleotide concentrations that were sufficiently high that free and total ligand concentrations were equal. The free dATP concentration at low total dATP concentrations is given by eq 11.

Measurements

DLS. Masses measured by DLS were fit to eq 12, using the values for $[R1]_t$, $[R1_2]_t$, $[R1_4]_t$, and $[R1_6]_t$ given in eqs 8a−e, 9a, or 9b, as appropriate.

Table 2: Equations for Measurements

DLS measurements

$$M_{obsd} = \frac{90\ \text{kDa}}{[R1]_T}([R1]_t + 4[R1_2]_t + 16[R1_4]_t + 36[R1_6]_t) \quad (12)$$

dATP binding

in the absence of a competing ligand

$$[A]_b = \sum_{i=0}^{2} i[R1_2L_i] + \sum_{i=0}^{4}\sum_{j=0}^{4}(i+j)[R1_{4a}L_iA'_j](1+K_{is}) + \sum_{i=0}^{6}\sum_{j=0}^{6}\sum_{k=0}^{6}(i+j+k)[R1_6L_iA'_jA''_k] \quad (13)$$

in the presence of competing dGTP (G)

$$[A]_b = \sum_{i=0}^{2-j}\sum_{j=0}^{2} j[R1_2G_iL_j] + \sum_{i=0}^{4-j}\sum_{j=0}^{4}\sum_{k=0}^{4}(j+k)[R1_{4a}G_iL_jA'_k](1+K_{is}) + \sum_{i=0}^{6-j}\sum_{j=0}^{6}\sum_{k=0}^{6}\sum_{l=0}^{6}(j+k+l)[R1_6G_iL_jA'_kA''_l] \quad (14)$$

in the presence of competing ATP (dATP = dA; ATP = A)

$$[dA]_b = \sum_{i=0}^{2}\sum_{j=0}^{2-j} i[R1_2dA_iA_j] + \sum_{i=0}^{4}\sum_{j=0}^{4-i}\sum_{k=0}^{4}\sum_{l=0}^{4-k}(i+k)[R1_{4a}dA_iA_jdA'_kA'_l](1+K_{is}) + \sum_{i=0}^{6}\sum_{j=0}^{6-i}\sum_{k=0}^{6}\sum_{l=0}^{6-k}\sum_{m=0}^{6}\sum_{n=0}^{6-m}(i+k+m)[R1_6dA_iA_jdA_k'A_l'dA_m''A_n''] \quad (15)$$

enzyme activity

UDP reductase

$$v = \left[\frac{\alpha(2+\alpha)}{(1+\alpha)^2[R1]_T}\right]\left[2k_d[R1_2]_t + 4\frac{k_d(1+K_{is}) + (k_{4a}+k_{4b}K_{is})\beta(2+\beta)}{(1+K_{is})(1+\beta)^2}[R1_4]_t + 6\frac{(k_{4b}+k_h\gamma)(2+\gamma)}{(1+\gamma)^2}[R1_6]_t\right] \quad (16)$$

ADP, GDP, or CDP reductase

$$v = \frac{1}{[R1]_T}\left[2k_d[R1_2]_t + 4\frac{k_d(1+K_{is}) + (k_{4a}+k_{4b}K_{is})\beta(2+\beta)}{(1+K_{is})(1+\beta)^2}[R1_4]_t + 6\frac{(k_{4b}+k_h\gamma)(2+\gamma)}{(1+\gamma)^2}[R1_6]_t\right] \quad (17)$$

dATP Binding. R1-bound dATP concentrations were fit for measurements made (a) in the absence of other nucleotides (eq 13), (b) in the presence of dGTP (eq 14, where G refers to dGTP), or (c) in the presence of ATP (eq 15, where A refers to ATP and dA refers to dATP).

RR Activity. Reductase activities, performed at saturating concentrations of $[R2_2]$ and substrate, were measured as functions of either ATP or dATP concentration. UDP reductase activity was fit to eq 16. ADP and GDP reductase activities were determined in the presence of saturating dTTP or dGTP, under which conditions the equation for enzyme activity simplifies from eq 16 to eq 17. CDP reductase activities were also fit to eq 17, based on the observation of appreciable CDP reductase in the absence of an s-site ligand; i.e., the $R2_2$ complex of the R1 dimer with the s-site empty is enzymatically active. Terms in $R2_2$ and substrate are omitted for simplicity, and rate constants k_d, k_{4a}, k_{4b}, and k_h are per monomeric R1 subunit. Equations 16 and 17 incorporate three important assumptions. First, that full activation of the R1 dimer results from binding to one s-site per dimer of the appropriate allosteric effector, evidence for which has been presented previously (*15*). Second, as with the s-site, binding to one a-site or h-site per R1 dimer confers the characteristic activity on both R1 subunits. The third is that the enzymatic activities of tetramers and hexamers are dependent on the nature of both a-site and h-site occupancies, respectively (see the Discussion).

Curve Fitting Procedures

DLS, activity, and binding data were fit using Igor Pro 3.16 (Wavemetrics, Oswego, OR). Simulated curves employed calculations at 200 equally spaced values of the independent variable, except that 10 000 equally spaced values were employed in fitting the dependence on dATP concentration of R1 DLS (Figure 3) and CDP reductase (Figure 9). Fitting of DLS and rate data as functions of either ATP or dATP concentration required graphical solutions of sixth-order equations. dATP binding data were fit using an iterative, self-consistent approach. Details of these procedures are available as Supporting Information.

RESULTS

ATP Induces Formation of R1 Dimers, Tetramers, and Hexamers

ATP effects on R1 oligomerization were measured by DLS, SE, and SV experiments. As shown by DLS measurements carried out at $[R1]_T = 7\ \mu M$ (Figure 1), ATP induces R1 hexamer formation (molecular mass of 540 kDa). Weight average molecular masses corresponding to the R1 dimer (180 kDa) and tetramer (360 kDa) are reached at ATP concentrations of 200 and 400 μM, respectively, with virtually full conversion to the hexamer (540 kDa) requiring 1−2 mM ATP.

ATP-induced formation of the hexamer was also shown by SE experiments (data not shown, Supporting Information). At 2 mM ATP, R1 sediments exclusively as a hexamer, with a molecular mass of 545 ± 5 kDa. By contrast, in the absence of ATP, R1 sediments as an equilibrium mixture of the monomer and dimer, with an apparent dissociation constant of $10^{-3.2\pm0.2}$ M, in reasonable accord with our previous estimate [$10^{-3.8\pm0.3}$ M (*15*)].

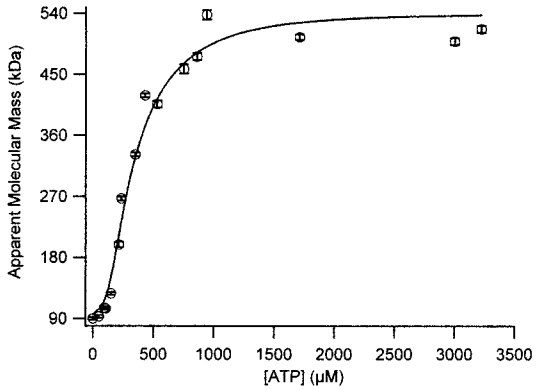

FIGURE 1: Dependence of R1 molecular mass on [ATP], as measured by DLS. [R1] = 7 μM. The solid line shows the best fit using eqs 8a−e and 12.

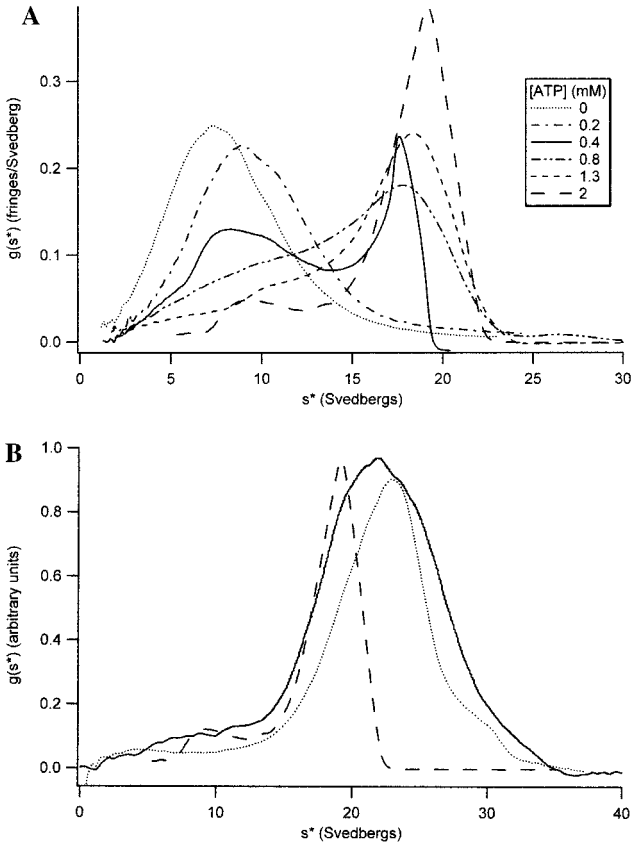

FIGURE 2: SV determination of R1 molecular mass. (A) [R1] = 8.2 μM with a varying ATP concentration. (B) R1 = 8.2 μM, and [ATP] = 2 mM (− − −). [R1] = 31 μM, and [ATP] = 2 mM (···). [R1] = 7 μM, [ATP] = 10 mM, and [R2] = 11.7 μM (—).

The dependence of R1 SV on ATP concentration (Figure 2A) clearly demonstrates the sequential formation of the dimer, tetramer, and hexamer. In experiments carried out at 8 μM R1, the *s* value of the dominant peak increases from 6.9 S, observed in the absence of added ATP and corresponding to the monomer, to ~9 S in the presence of 200 μM ATP, corresponding to substantial dimer formation. It continues to increase with increasing ATP concentrations, passing through 17 S corresponding to tetramer, at 800 μM, and reaching a value of 19.5 S, reflecting a mixture of the tetramer and hexamer, at 2 mM ATP. Increasing the R1 concentration to 31 μM yields a species sedimenting with an *s* value of 23 S in the presence of 2 mM ATP (Figure 2B), corresponding to full hexamer formation.[2] That full hexamer formation at 1−2 mM ATP requires a higher R1 concentration in the SV experiments than in the DLS experiments may reflect R1 concentration gradient formation during sedimentation, with attendant dissociation in regions of lower concentrations. Pressure-induced dissociation may also be a factor. Finally, addition of $R2_2$ to a predominantly hexameric R1 solution increases the measured *s* value of the dominant species in solution to 23 S and broadens the peak, with virtually all protein sedimenting between 17 and 30 S, and little protein sedimenting below 15 S (Figure 2B). This result demonstrates that $R2_2$ binds to $R1_6$ without inducing $R1_6$ dissociation.

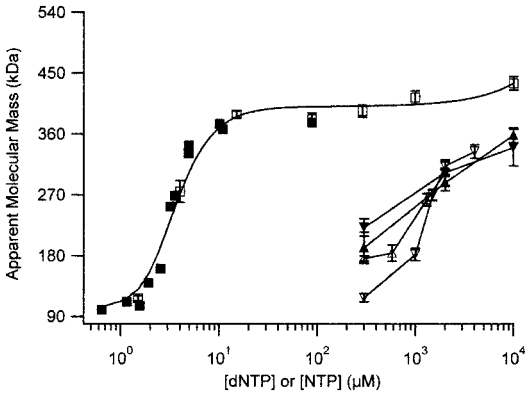

FIGURE 3: Dependence of R1 molecular mass on nucleotide triphosphate concentration as measured by DLS. [dATP]: [R1] = 7.3 (■) and 8.0 μM (□). The solid line shows the best fit using eqs 8a−e, 11, and 12. [UTP] (△), [dTTP] (▲), [GTP] (▽), or [dGTP] (▼): [R1] = 10 μM.

dATP Induces Formation of R1 Dimers, Tetramers, and, to a Small Extent, Hexamers

Like ATP, added dATP induces R1 aggregation as measured by DLS, with the difference that dATP concentrations required for dimer and tetramer formation are much lower (2 and 8 μM, respectively) (Figure 3). There is a long plateau region (20−300 μM dATP) at an apparent molecular mass (385 kDa) that is somewhat larger than that expected for the R1 tetramer and a gradual increase to >435 kDa, as the dATP concentration is increased to 10 mM. These latter results reflect a small amount of hexamer formation, the extent of which is increased at very high dATP concentrations. dATP-induced R1 tetramer formation is also demonstrated by an SV experiment (data not shown) in which addition of 1 mM dATP leads to a clear peak centered at 16 S.

Specificity of Ligand-Induced R1 Oligomerization

Results of surveying a variety of ligands for their abilities to induce R1 oligomerization, as measured by DLS, are summarized in Table 3. These results, coupled with the results presented in Figure 3, lead to two important conclusions. First, while dATP is unique in inducing tetramer formation at low concentrations (<10 μM), a number of other

[2] Using an *s* value for the R1 monomer of 6.9, and assuming different oligomeric forms of R1 have similar globular shapes, allows calculation of *s* values for the dimer, tetramer, and hexamer of 10.9, 17.4, and 22.8, using the relationship $s_1/s_2 = (M_1/M_2)^{2/3}$ (*17*).

Table 3: Effects on R1 Apparent Masses

added compd	apparent mass (kDa)[a]	added compd	apparent mass (kDa)[a]
5.0 mM PO_4	85	4.3 mM ADP	332
4.1 mM AMP	162	5.0 mM P_3O_{10}	160
5.0 mM P_2O_7	88	5.0 mM ddATP	468

[a] As measured by DLS, [R1] = 10 μM.

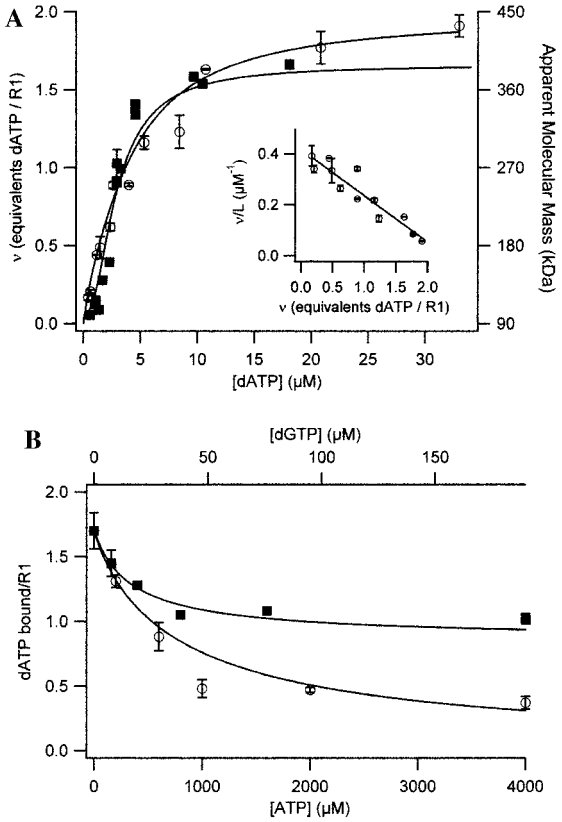

FIGURE 4: (A) dATP binding to the R1−R2 complex in the absence of other ligands (○), overlaid with DLS data (■) reprised from Figure 3. The inset shows binding data plotted in Scatchard form. [R1] = 5.6 μM, and [R2] = 13 μM with a varying dATP concentration. The solid line shows the best fit using eqs 8a−e, 11, and 13. (B) dATP binding to the R1−R2 complex in the presence of competing dGTP (■) and ATP (○). [R1] = 5.6 μM. [R2] = 30 μM. [dATP] = 21.4 μM with a varying dGTP or ATP concentration. dGTP competition data was fit using eqs 9a and 14. ATP competition data were fit using eqs 10 and 15, giving fitted values of K_L for dGTP (1.4 ± 0.1 μM) and of K_L (40 ± 8 μM) and $K_{A'}$ (90 ± 16 μM) for ATP. All points are the average of duplicate measurements ± the average deviation.

ligands, in addition to ATP, do induce at least partial tetramer formation at higher concentrations, including dTTP, dGTP, UTP, GTP, ADP, and ddATP. Second, ATP is unique in its ability to induce virtually full R1 hexamer formation at a concentration of 1−2 mM. Of the other ligands that were tested, only dATP and ddATP show any evidence of being able to induce hexamer formation, but for each of these, concentrations ≫5 mM would be required for full hexamer formation. Interestingly, even added AMP or inorganic tripolyphosphate is able to induce dimerization.

dATP Binding to the R1R2 Complex

dATP binds to two high-affinity sites per R1 monomer in the presence of saturating $R2_2$ (see below), corresponding

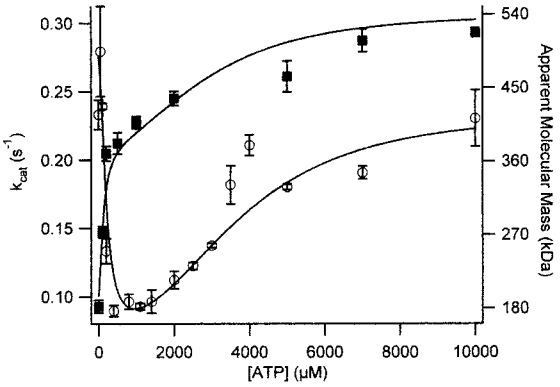

FIGURE 5: Dependence of dTTP-dependent GDP reductase and R1 molecular mass on ATP concentration. All solutions contained 300 μM dTTP, 100 μM GDP, and varying ATP concentrations as shown. Solutions for measuring GDP reductase (○) also contained 1.2 μM R1 and 2.0 μM R2. Each point is the average of two to eight measurements ± the average deviation. Solutions for measuring the molecular mass of R1 by DLS (■) also contained 5.7 μM R1. The two data sets were fit simultaneously using eqs 9b, 12, and 17.

to the s- and a-sites (Figure 4A). Overlaying the binding data in Figure 4A with the DLS data from Figure 3 demonstrates clear correlations between dimer and tetramer formation and the binding of the first and second dATP equivalents, respectively. In agreement with Reichard et al. (*4*), addition of a saturating amount of dGTP leads to a loss of one dATP binding site (the s-site) per R1 monomer, whereas ATP competes for both s- and a-sites (Figure 4B).

ATP Effects on RR Activity

GDP and ADP Reductase. Using the standard enzyme activity assay conditions described in Experimental Procedures, dTTP-dependent GDP reductase specific activity displays a biphasic dependence on ATP concentration, falling from 0.28 to ∼0.09 s^{-1} as the ATP concentration is increased to 800 μM, and then rebounding as the ATP concentration is further increased, reaching a plateau value of 0.25 s^{-1} at 5−10 mM ATP (Figure 5). Overlaid with the activity results are the results of DLS experiments performed under the same conditions as the activity assay, except lacking $R2_2$. These results provide strong support for two important aspects of Scheme 1.

First, they clearly demonstrate ATP binding to two different sites on R1 in addition to the s-site to which dTTP is bound, constituting the first strong evidence for three allosteric sites on R1. The reasoning here is as follows. The biphasic character of the curve constitutes evidence for ATP binding to two sites. However, since dTTP binding to the s-site is essential for GDP reduction, the high concentrations of ATP that activate GDP reduction must be insufficient to displace dTTP from the s-site (also, see below). Therefore, ATP binds to two allosteric sites in addition to the s-site.

Second, the range of ATP concentrations giving first inactivation and then activation of GDP reductase strongly overlaps the range of ATP concentrations leading to R1 tetramer and hexamer formation, respectively, clearly linking R1 tetramer and hexamer formation to the loss and regain of enzymatic activity. R1 is a dimer in the presence of 300 μM dTTP (*15*). From the shape of the activity−ATP concentration curve, it is clear that the $R2_2$ complexes of

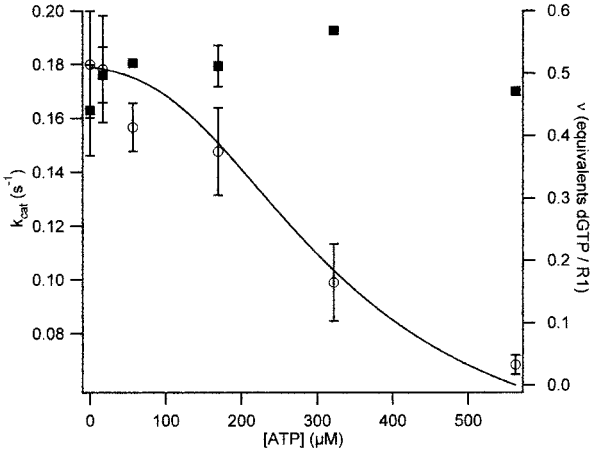

FIGURE 6: Dependence of dGTP-dependent ADP reductase and dGTP binding on ATP concentration. All solutions contained 0.86 μM R1, 6.2 μM R2, 2.1 μM [^{3}H]dGTP, 350 μM [^{14}C]ADP, and varying ATP concentrations. Levels of ADP reductase (○) and dGTP binding (■) were determined on aliquots taken from the same solution. Activity data are fit using eqs 9b and 17.

both the R1 dimer and hexamer have similar activities, whereas the $R2_2$ complex of the R1 tetramer has considerably lower activity. Interestingly, comparison of the DLS data in Figures 1 and 5 shows that an approximately 5-fold higher concentration of ATP (5−10 mM) is needed to induce full R1 hexamer formation when measurements are carried out in the presence of dTTP and GDP, i.e., under conditions paralleling those used in activity assays.

dGTP-dependent ADP reductase also shows inhibition by ATP up to a concentration of 570 μM (Figure 6). This experiment was conducted at a limiting dGTP concentration, corresponding to just under half-saturation of the s-site, to provide a direct test of whether ATP displaces dGTP from the s-site. As little if any such displacement occurs, ATP inhibition of ADP reductase cannot be due to displacement of dGTP from the s-site. Since dGTP and dTTP have very similar affinities for the s-site (*15*), the results depicted in Figure 6 provide additional evidence that ATP inhibition of GDP reductase (Figure 5) is also not a consequence of displacement of dTTP from the s-site.

CDP and UDP Reductase. CDP is the only one of the four ribonucleoside diphosphate substrates that is reduced by RR with a significant activity, even in the absence of allosteric effectors, with a K_m of 120 ± 40 μM and a k_{cat} of 0.047 ± 0.005 s^{-1} (data not shown). CDP reductase specific activity has a triphasic dependence on ATP concentration, increasing to 0.26 s^{-1} as the ATP concentration is increased to 0.2 mM, falling to 0.16 s^{-1} with a further increase in ATP concentration to 1 mM, and increasing again to 0.29 s^{-1} as the ATP concentration is increased to 4 mM (Figure 7A). This behavior is fully consistent with Scheme 1. Activation at low ATP concentrations is due to an increased level of R1 dimer formation on ATP binding to the s-site, and the subsequent loss and regain of activity as the ATP concentration is increased further parallels the GDP reductase results (Figure 5). As in Figure 5, the activity results are overlaid with the results of DLS experiments performed under the same conditions as the activity assay, except lacking $R2_2$. This overlay shows a clear correlation between R1 dimer, tetramer, and hexamer formation and increased, decreased, and re-increased activity, respectively. In the presence of 3 mM ATP, the steady-state parameters for CDP reduction show a much reduced K_m (2.0 ± 0.3 μM) and an increased k_{cat} (0.30 ± 0.02 s^{-1}) vis-à-vis no added ATP (data not shown).

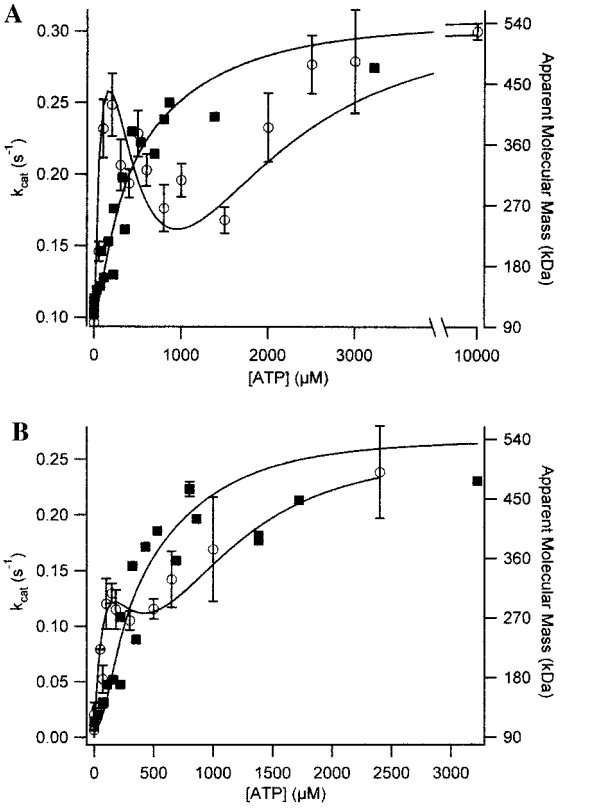

FIGURE 7: Dependence of pyrimidine diphosphate reductase and R1 molecular mass on ATP concentration. (A) All solutions contained 1 mM CDP and a varying ATP concentration as shown. Solutions for measuring CDP reductase (○) also contained 1.2 μM R1 and 2.0 μM R2. Each point is the average of two to eight measurements ± the average deviation. Solutions for measuring the molecular mass of R1 by DLS (■) also contained 7 μM R1. (B) Solutions for measuring UDP reductase (○) contained 1.6 μM R1, 6.6 μM R2, 810 μM UDP, and a varying ATP concentration. Solutions for measuring the molecular mass of R1 by DLS (■) contained 7 μM R1, 1 mM UDP, and a varying ATP concentration. The two data sets in panel A were fit simultaneously, using eqs 8a−e, 12, and 17. The data sets in panel B were fit simultaneously, using eqs 8a−e, 12, and 16.

UDP reductase also shows a similar triphasic dependence on ATP concentration (Figure 7B), and the overlay with the results of DLS experiments again demonstrates the correlation between R1 dimer, tetramer, and hexamer formation and increased, decreased, and re-increased activity, respectively. In the presence of 3 mM ATP, the K_m (6.4 ± 1.5 μM) and k_{cat} (0.25 ± 0.02 s^{-1}) values for UDP reductase are similar to those obtained for CDP reductase (data not shown).

dATP Effects on RR Activity

GDP and ADP Reductase. dATP inhibits both dTTP-dependent GDP reductase and dGTP-dependent ADP reductase at similar concentrations (Figure 8). Overlaying the activity data with the results of DLS experiments performed in the presence of a saturating amount of dTTP shows a clear correlation between the loss of activity and tetramer formation.

CDP and UDP Reductase. CDP reductase shows a biphasic response to increasing dATP concentrations, being

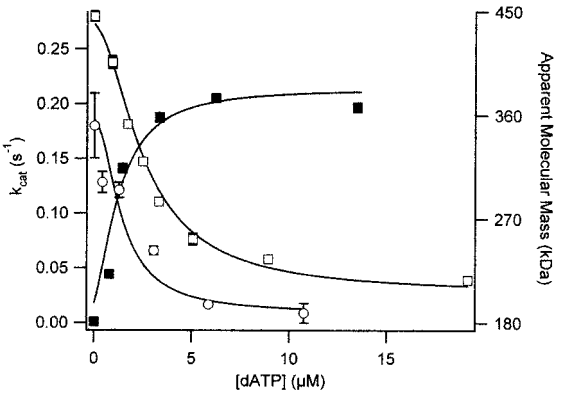

FIGURE 8: Dependence of dNTP-dependent purine reductase and R1 molecular mass on dATP concentration. Solutions for measuring GDP (□) or ADP (○) reductase contained 2.0 μM R1, 20 μM R2, 100 μM dTTP, and 1 mM GDP or 1.2 μM R1, 4.8 μM R2, 2.1 μM dGTP, and 350 μM ADP, respectively, and a varying dATP concentration. Solutions for measuring the molecular mass of R1 by DLS (■) contained 6.1 μM R1, 0.98 mM dTTP, and a varying dATP concentration. Each reductase data set was fit using eqs 9b, 11, and 17. DLS data were fit using eqs 9b, 11, and 12.

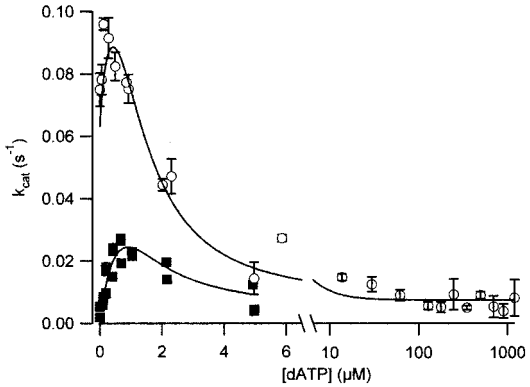

FIGURE 9: Dependence of pyrimidine diphosphate reductase on dATP concentration. Solutions for measuring CDP reductase (○) contained 1.2 μM R1, 4.0 μM R2, 1.1 mM CDP, and a varying dATP concentration. Data were fit using eqs 8a−e, 11, and 17. Solutions for measuring UDP reductase (■) contained 1.3 μM R1, 5.6 μM R2, 820 μM UDP, and a varying dATP concentration. Data were fit using eqs 8a−e, 11, and 16.

activated by low dATP concentrations, corresponding to the binding of dATP to the s-site, followed by inhibition at higher dATP concentrations, corresponding to dATP binding to the a-site (Figure 9). These two phases thus resemble what is found for the first two phases of the response of CDP reductase to increasing ATP concentrations (Figure 7A) except that they occur at a very much lower (∼100-fold) dATP concentration, corresponding closely to the dATP concentrations required for $R1_2$ and $R1_4$ formation (Figure 3). In addition, the maximum observed velocities are clearly lower. However, unlike ATP, no activation is seen on further increasing the dATP concentration to as high as 1 mM. A similar biphasic pattern is seen for UDP reductase as a function of dATP concentration (Figure 9), but the activation phase is more pronounced, since RR has no UDP reductase activity in the absence of ATP or dATP.

dTTP and dGTP Effects on RR Activity

Earlier, we showed that dTTP and dGTP concentrations of 10 μM were sufficient to fully activate the GDP and ADP reductase activities of RR (*15*). The DLS results in Figure 3 prompted us to investigate whether the dTTP- and dGTP-induced formation of R1 tetramer had any consequence for GDP and ADP reductase. Little or no change was found for either assay over the range of 0.3−2 mM (data not shown). Even increasing the concentration to 10 mM caused only modest decreases in activity (17% for dTTP-induced GDP reductase and 46% for dGTP-induced ADP reductase) which could well be due to competition for substrate binding.

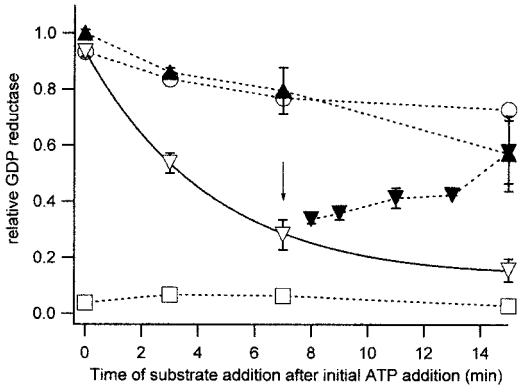

FIGURE 10: Preincubation effects on dTTP-dependent GDP reductase. Reaction mixtures containing 1.2 μM R1, 2.0 μM R2, and 300 μM dTTP were preincubated for the times shown, in the absence of added nucleotide triphosphate (○) or in the presence of 0.5 mM ATP (▽), 10 mM ATP (▲), or 20 μM dATP (□). The reaction was initiated on addition of 700 μM GDP, after which GDP reductase was determined in the usual manner. For the ATP-jump experiment (▼), preincubation was carried out at 0.5 mM ATP for 7 min, after which the solution was brought to 10 mM ATP (addition indicated by arrow) and preincubation was continued for additional times prior to addition of 700 μM GDP. Shown are total incubation times prior to substrate addition. Data for the experiments carried out in the absence of added nucleotide triphosphate or in the presence of 10 mM ATP were fit with a first-order rate constant of 0.026 ± 0.005 s^{-1} for ATP-independent inactivation of enzymatic activity. Data for the experiment carried out in the presence of 0.5 mM ATP were fit to two parallel first-order rate constants, 0.026 s^{-1} as described above and 0.24 ± 0.03 s^{-1} for ATP-dependent inactivation of enzymatic activity. Data for the ATP-jump experiment were fit to a first-order rate constant of 0.18 ± 0.14 s^{-1}.

$R1_4$ Isomerization and the Effect of Preincubation on ATP Inhibition of GDP Reductase

Measurements of reductase activity, as presented in Figures 5−9, were obtained using the standard assay, in which all of the reaction components except substrate are preincubated for 7 min prior to initiation of the reaction with substrate. Shown in Figure 10 is the effect of varying the time of preincubation (0−15 min) on dTTP-dependent GDP reduction, in the absence of ATP and at ATP concentrations equal to 0.5 and 10 mM. Under the first and last of these conditions, R1 is in the form of a dimer and hexamer, respectively, whereas 0.5 mM ATP gives close to the maximum amount of tetramer (Figures 1, 2A, and 5). Although activity falls as a function of preincubation time for all three conditions, the rate of activity loss is much faster at 0.5 mM ATP. We interpret these results as an indication that there are two inactivation processes. The slower one, which we term ATP-independent inactivation, is present under all three conditions, has a first-order rate constant of 0.026 ± 0.005 min^{-1}, and may arise from effects of the R2

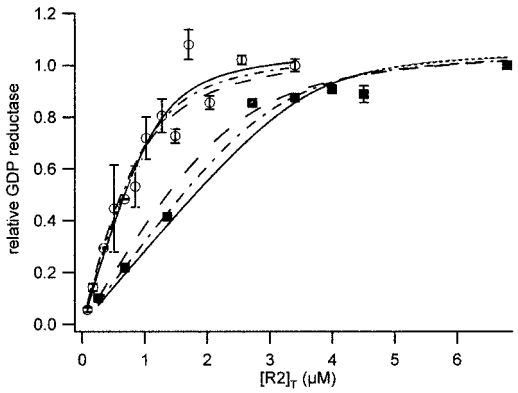

FIGURE 11: Dependence of dTTP-dependent GDP reductase on $R2_2$ concentration. R2 was added in the amounts shown to 300 μM dTTP, 10 mM ATP, and either 1.2 μM R1 (○) or 3.6 μM R1 (■). All of the data were fit to eq 18 either treating *n* as a parameter to be fit [yielding $n = 2.6 \pm 0.3$, $K_d = 96 \pm 46$ nM (−•−)] or setting *n* equal to 3 [$K_d = 66 \pm 36$ nM (—)] or 2 [$K_d = 145 \pm 48$ nM (− − −)].

tyrosyl free radical. The faster process, which we term ATP-dependent inactivation, only comes into play at 0.5 mM ATP, and has a first-order rate constant of 0.24 ± 0.03 min^{-1}. Also shown in Figure 10 are the results of an "ATP-jump" experiment. Here, preincubation was carried out at 0.5 mM ATP for 7 min, and a sample aliquot was withdrawn for assay. The remaining reaction mixture was brought to 10 mM ATP, and aliquots were assayed over time. Assay prior to the ATP jump gave the expected large activity loss, whereas following the jump, activity increased over an 8 min period to that expected for a 15 min preincubation with 10 mM ATP. The rate constant for the reactivation of reductase was estimated to be 0.18 ± 0.14 min^{-1}, within experimental error of that for ATP-dependent inactivation.

These results provide the basis for the inclusion of the reversible isomerization of $R1_{4a}$ to $R1_{4b}$ in Scheme 1. On the basis of the rate constants presented above, the net rate constant for $R1_{4a}-R1_{4b}$ equilibration is ~0.2 min^{-1}. According to Scheme 1, enzymatically active $R1_2$ is rapidly converted to active $R1_6$ via $R1_{4a}$. This was shown directly by a MALLS experiment (data not shown) demonstrating that $R1_6$ formation is complete in <2 min on addition of 5 mM ATP to a reaction mixture containing 4 μM R1 and 300 μM dTTP. At 0.5 mM ATP, the equilibrium concentration of $R1_{4b}$, which has very low specific activity, is considerable. As a result, during a preincubation period of 7 min (approximately two half-lives for $R1_{4a}-R1_{4b}$ equilibration), $R1_{4b}$ accumulates at the expense of $R1_2$ and $R1_6$, and activity decreases. By contrast, in the absence of preincubation, $R1_{4b}$ has no time to accumulate, and activity remains high. As the equilibrium concentration of $R1_{4b}$ is very low either in the absence of ATP or in the presence of 10 mM ATP, preincubation has little effect on activity, except for ATP-independent inactivation.

In contrast to the ATP effects, the activity loss resulting from addition of 20 μM dATP is rapid, showing no dependence on the time of preincubation prior to substrate addition. This indicates either that $R1_{4a}-R1_{4b}$ equilibration is more rapid in the presence of dATP than in the presence of ATP or else that the $R2_2$ complex of $R1_{4a}$ has little enzymatic activity (see the Discussion).

Stoichiometry of $R2_2$ Activation of $R1_6$

To determine the stoichiometry of $R2_2$ needed for full activation of the R1 hexamer, formed in the presence of 10 mM ATP (Figure 5), we measured the dependence of dTTP-dependent GDP reductase activity on the $R2_2$ concentration at two fixed R1 concentrations (Figure 11). The results obtained were fit to eq 18, in which *V* is the velocity at a saturating $R2_2$ concentration. Equation 18 is derived assuming that (a) *n* $R2_2$ dimers are bound per R1 hexamer with a single intrinsic dissociation constant, K_d, and (b) observed enzyme activity, v, is proportional to the number of $R2_2$ dimers bound per R1 hexamer. Best fit values were obtained for an *n* of 2.6 ± 0.3 and a K_d of 96 ± 46 nM. As shown, reasonable fits to the data were also obtained if *n* were fixed at 3 or 2, giving a K_d value of 66 ± 36 or 145 ± 48 nM, respectively. On the other hand, an *n* of 1 gave much poorer fits (data not shown).

$$v = \frac{V}{2n[R1_6]_t}[K_d + n[R1_6]_t + [R2_2]_t + \sqrt{(K_d + n[R1_6]_t - [R2_2]_t)^2 + 4K_d[R2_2]_t}] \quad (18)$$

Earlier, we determined a K_d for $R2_2$ activation of the R1 dimer, formed in the presence of dTTP and GDP, of 21 ± 14 nM (*15*). This value is within experimental error of that determined assuming an *n* of 3. Combining both sets of results, we consider the most likely fully active form of enzyme at a high ATP concentration (10 mM) to be the heterohexamer, $R1_6R2_6$, although we are unable to rule out fully active forms of the enzyme having an R2:R1 ratio of somewhat less than 1. Previously, Ingemarson and Thelander (*18*) determined an R2:R1 binding stoichiometry of 1.3 at 5 mM ATP, using a biosensor technique with immobilized R2. We take this value to be an upper limit, since some inactivation of R2 on immobilization is possible.

DISCUSSION

Scheme 1 provides a simple yet complete framework for understanding the apparently complex modulation of RR enzymatic activity by ATP and dATP, as demonstrated by our ability to fit data collected in a wide variety of experiments with a limited number of parameters. Below, we first consider the evaluation of pertinent equilibrium and rate constants and go on to discuss the implications of the values obtained for (a) site−site interactions within mRR and their consequences for enzymatic activity and (b) in vivo activity of mRR. We conclude with consideration of a structural model that rationalizes specific features of Scheme 1.

Evaluation of Equilibrium and Rate Constants. Fitting the results in Figures 1 and 3−9 to eqs 12−17, generated from Scheme 1, required evaluation of the seven equilibrium constants defined by eqs 1−7 (Table 1). Of these, only one, K_o, had a marked dependence on the presence of $R2_2$, having values of 170 and 5 μM in the absence and presence of (saturating) $R2_2$, respectively, as determined previously (*15*). All other equilibrium constants were evaluated assuming that the presence of $R2_2$ had no effect, with one minor exception, noted below. Thus, for example, single values for each of the K_L, $K_{A'}$, and $K_{A''}$ constants describing ATP binding in

Table 4: Dissociation Constants (μM) for ATP and dATP[a]

ligand		no addition	with dTTP and GDP	with dGTP and ADP	with CDP	with UDP
ATP	K_L	94 ± 2	−	−	25 ± 1	44 ± 1 **61 ± 1**
	$K_{A'}$	94 ± 2	140 ± 10	110 ± 10	300 ± 10	210 ± 10 **160 ± 10**
	$K_{A''}$	1100 ± 100	4200 ± 100	not determined	1800 ± 100 **2200 ± 100**	1200 ± 100
	Figure	1	5	6	7	7
dATP	K_L	1.1 ± 0.2/0.94 ± 0.01	−	−	0.66 ± 0.02	0.9 ± 0.1
	$K_{A'}$	1.1 ± 0.2/2.3 ± 0.1	0.96 ± 0.01 (1.7 ± 0.1)[b]	0.7 ± 0.3	0.30 ± 0.01	0.28 ± 0.03
	Figure	3/4A	8	8	9	9

[a] Fitted values shown are for assumption I; values in bold are for assumption II which differ from those calculated for assumption I by >10%. [b] No added GDP.

the presence of CDP gave adequate fits to both the DLS (without $R2_2$) and activity (with $R2_2$) results (Figure 7A).

Our results indicate little accumulation of $R1_{4a}$ in any of the reported experiments, so we were unable to estimate k_{4a}. As a result, fitting calculations were carried out for each of two limiting assumptions: (I) that both tetrameric forms have low activity ($k_{4a} = k_{4b}$), which would be consistent with the rapid activity loss seen on addition of dATP (Figure 10), or (II) that $R1_{4a}$ displays full enzymatic activity [$k_{4a} = (k_d + k_h)/2$]. As defined, K_t, K_h, and K_{is} are independent of R1 ligands, and consistent with these definitions, all of the data in Figures 1 and 3−9 could be adequately fit with single values of each of these constants. These values, which were different for assumption I and assumption II (in parentheses), were as follows: $K_t = 2.0 \pm 0.1$ mM (5.9 ± 0.1 mM), $K_h = 6 \pm 1$ μM (1.7 ± 0.1 μM), and $K_{is} = 10$ (40).[3] Despite these differences, it is clear that, at equilibrium, the overall distribution of R1 among the major species in solution is essentially the same for assumptions I and II, since $[R1_2]^2/[R1_{4b}]$ is equal to K_{is}/K_t and $([R1_2][R1_{4b}])/[R1_6]$ is equal to K_hK_{is}. Accordingly, values of K_L, $K_{A'}$, and $K_{A''}$ for ATP or of K_L and $K_{A'}$ for dATP (Table 4)[4] were almost the same for either assumption I or assumption II. A comparison of K_L and $K_{A'}$ values for dATP binding in the absence (DLS, Figure 3) or presence (equilibrium dialysis, Figure 4A) of $R2_2$ shows that added $R2_2$ had no effect on K_L and only a minor (2-fold) effect on $K_{A'}$.

For the most part, the catalytic efficiencies of the active forms of mRR are quite similar (Table 5). Thus, the k_d values for the GDP/dTTP, ADP/dGTP, CDP/ATP, UDP/ATP, and CDP/dATP catalytic pairs and the k_h values for ATP activation of GDP, CDP, and UDP all fall within a narrow range (0.16−0.29 s^{-1}). The exception is the k_d value for the UDP/dATP pair, which is notably lower (0.08 s^{-1}). The general similarity of rate constants suggests that once a conformation at the active site that is appropriate for ribose reduction is achieved through s-site and, as needed, h-site binding, a common step, such as cystine formation within mR1 (*19*), becomes fully or partially rate-determining.

[3] Although curve fitting of reductase activity is carried out assuming full equilibration among $R1_2$, $R1_{4a}$, $R1_{4b}$, and $R1_6$, the standard preincubation time of 7 min corresponds to two half-lives for $R1_{4a}$−$R1_{4b}$ equilibration. As a result, values for K_{is} are systematically slightly underestimated. However, since only a lower limit of K_{is} could be estimated, this error has little practical consequence.

[4] The fitted value of $K_{A''}$ for dATP (Figure 3) was so high (61 ± 7 mM) that h-site binding of dATP could be safely ignored.

Table 5: Reductase Rate Constants (s^{-1})[a]

rate constant	GDP	ADP	CDP	UDP
k_d	0.28	0.18	0.29[b]/0.25[c]	0.16[b]/0.08[c]
k_{4b}[d]	0.028 **0.022**	0.008 **0.006**		
k_h[b]	0.25	ND[e]	0.30	0.26

[a] Fitted values shown are for assumption I; values in bold are for assumption II which differ from those calculated for assumption I by >10%. [b] Values in the presence of ATP. [c] Values in the presence of dATP. [d] Values are the same in the presence of ATP or dATP. [e] Not determined.

Site−Site Interactions within mRR and Their Consequences for Enzymatic Activity. Three publications have recently appeared in which allosteric effector binding to murine RR was measured (*4*, *14*, *15*). These studies are consistent with the present work in showing that dATP, dTTP, dGTP, and ATP compete with each other for binding to the s-site, while only ATP and dATP bind to the a-site, that dGTP and dTTP bind to the s-site with comparable affinities, and that the ATP affinity for both sites is much lower (~2 orders of magnitude) than the dATP affinity (Table 4). However, the values of the dissociation constants for dATP binding to R1 in the absence of other ligands, measured in this work and two of the other studies, each differ from one another. Thus, we find that K_L and $K_{A'}$ values are similar, both falling in the range of 0.9−2.3 μM, whether measured in the presence or absence of $R2_2$ (Table 4). By comparison, as measured in the absence of $R2_2$, Reichard et al. (*4*) report dissociation constants of 0.07 and 1.5 μM, whereas Chimploy and Mathews (*14*) report values of 12.6 and 54 μM. The reasons for these differences, which are obviously more pronounced with the latter study, are unclear. However, it is worth noting that the mR1 used in our studies was purified with a peptide affinity column, whereas the other studies employed a dATP affinity column, requiring high concentrations of ATP for protein elution.

Allosteric effects on activity may be exerted on either k_{cat} or substrate binding affinity, with thermodynamics requiring that the latter effects be reciprocal. Examination of substrate effects on allosteric binding to the s-, a-, and h-sites (Table 4) shows them to be modest, reinforcing the notion that allosteric effects on RR activity are principally exerted on k_{cat} and depend on which ligand occupies the allosteric site.

There has long been clear evidence for cooperative interaction between an NDP substrate bound to the active site and the allosteric ligand bound to the s-site that activates reduction of that NDP (*20*). In our earlier study on the purine

reductase activity of the $R1_2R2_2$ complex (*15*), we measured positive cooperative heterotropic binding effects (e.g., GDP effects on dTTP binding) of 2−4-fold. Similar positive heterotropic effects are now also seen for CDP and UDP on s-site binding (decreased K_L) of ATP and dATP, although the effects are smaller for dATP (Table 4).

The situation with the a-site is more complex. As with the s-site, the nature of the ligand occupying the a-site determines enzyme activity, with both ATP and dATP inducing formation of the low-activity R1 tetramer, whereas either dGTP or dTTP can induce R1 tetramer formation (Figure 3) without inhibiting RR enzymatic activity. However, substrate binding has more varying effects on a-site binding than on s-site binding. Thus, whereas either the dTTP/GDP or dGTP/ADP pair has little or no clear effect on $K_{A'}$ for either ATP or dATP, UDP and CDP both increase the $K_{A'}$ for ATP (2−3-fold) while decreasing the $K_{A'}$ for dATP (2.5−8-fold). The effects of CDP and UDP on dATP binding have the consequence that, in the presence of either, K_L is greater than $K_{A'}$. As a result, the maximum dimer concentration induced as a function of dATP concentration is much lower than as a function of ATP concentration. This accounts for the much lower maximum velocities of CDP and UDP reductase observed as a function of dATP concentration (Figure 9) versus those seen as a function of ATP concentration (Figure 7), despite k_d values that are either similar (CDP reductase) or only 2-fold different (UDP reductase).

Concluding our consideration of substrate interaction with allosteric sites, the observation that the small amount of hexamer formed at high dATP concentrations (Figure 3) displays no enhanced activity (Figure 9) permits the suggestion that the enzymatic activity of the hexamer depends on ATP occupancy of the h-site. This is clearly a k_{cat} effect, since substrate effects on ATP binding to the h-site ($K_{A''}$) range from none at all (UDP) to negative [CDP (2-fold) and dTTP/GDP (4-fold)].

Last, the limited information that is available about the interaction of allosteric sites with one another comes from our studies of dGTP and ATP effects on dATP binding. The competitive curves (Figure 4B) gave fitted values of K_L for dGTP (1.4 ± 0.1 μM) and of K_L (40 ± 8 μM) and $K_{A'}$ (90 ± 16 μM) for ATP that are quite similar to those measured directly either by Scott et al. (*15*) [$K_{L(dGTP)} = 1.4 \pm 0.3$ μM] or by DLS (Table 4). These similarities suggest little interaction between dATP bound in the a-site and whatever ligand occupies the s-site.

In Vivo Activity of mRR. Comparison of the results presented in this paper with what is known about the cellular concentrations of mRR allosteric effectors and substrates leads to the conclusion that ATP binding to the h-site is crucial for controlling mRR activity in vivo and demonstrates an interesting correlation between in vivo NDP concentrations and relative rates of NDP reduction.

The concentration ranges found in mammalian cells for the allosteric effectors of mRR are as follows: 0.7−89 μM dTTP, 0.4−15 μM dGTP, 1−60 μM dATP, and 0.5−10 mM ATP (*21*, *22*). As a consequence, the allosteric s- and a-sites should be fully saturated in vivo, and the oligomeric forms of R1 present in the cell should be principally distributed among $R1_{4b}$, having low enzymatic activity when complexed with $R2_2$, and $R1_6$, having high enzymatic activity when complexed with $R2_2$. In these complexes, the s-site will be occupied by one of the four allosteric ligands, the a-site will be occupied by either ATP or dATP, and the h-site will be either occupied by ATP or empty. Neither R1 tetramer formation induced by dGTP or dTTP nor the very weak binding of dATP to the h-site (Figure 3) is physiologically relevant.

Table 6: Catalytic Properties of Mammalian RR

substrate	k_{cat}[a]	K_m (μM)	relative k_{cat}/K_m (murine)	relative k_{cat}/K_m (others)[d]	relative in vivo concentration[e]
ADP	0.18	12 ± 1	0.10[b]	0.045−0.73	1.00
GDP	0.28	4.9	0.38[b]	0.14−0.47	0.27 ± 0.20
CDP	0.30	2.0 ± 0.3	1.00[c]	1.00	0.04 ± 0.03
UDP	0.25	6.4	0.26[c]	0.13−0.23	0.15 ± 0.06

[a] Per R1 monomer. [b] From ref *15*. [c] From this work. [d] Calf thymus (*9*), Novikoff hepatoma (*34*), Ehrlich tumor (*36*), and Molt-4F (*10*). [e] Average for eight mammalian cells (±standard deviation); human eosinophils, erythrocytes, lymphocytes, monocytes, and neutrophils (*36*), rat liver and hepatoma (*37*), and mouse leukemia (*38*).

Binding of ATP to the h-site mediates the interconversion of $R1_{4b}$ and $R1_6$, and the values of the dissociation constant for dissociation of ATP from the h-site ($K_{A''}$) fall within the range of physiological ATP concentrations. It would thus appear that ATP binding to the h-site plays an important role in coupling the rate of DNA biosynthesis, as determined by total RR activity, with the energetic state of the cell. Such coupling should be modulated by the effectors dGTP or dTTP and the NDP substrates, via their effects on $K_{A''}$ (Table 4).

Collected in Table 6 are values for k_{cat} and K_m that have determined in this paper and by Scott et al. (*15*) for each of the four NDP substrates and murine ribonucleotide reductase, under conditions corresponding to maximum reductase activities. Displayed alongside the resulting normalized k_{cat}/K_m values are corresponding ranges of values reported for RRs from other mammalian sources, along with the normalized concentrations of each of the four substrates in several mammalian cells. The results for the murine enzyme show a striking inverse correlation of k_{cat}/K_m and in vivo NDP concentration. For instance, k_{cat}/K_m for CDP reductase is 10-fold greater than for ADP reductase and the ADP concentration is on average 25-fold higher than the CDP concentration, whereas for both measures, UDP and GDP fall between the extremes. Such an inverse correlation, suggestive of an enzyme that has been designed to produce dNDPs in a ratio reflective of that organism's genome [the A/T:G/C ratio in mammals is 1.4 (*23*)], has previously been found for RR from T4 bacteriophage (*24*). For the other mammalian RRs, the correlation is roughly maintained for CDP, UDP, and GDP, but the relative k_{cat}/K_m values for ADP fall over a range that is too wide to allow a clear conclusion, being much higher for RRs from calf thymus and Ehrlich tumor cells [0.68 (*9*) and 0.73 (*25*), respectively] than for RRs from Novikoff hepatoma cells [0.045 (*26*)] or mouse (0.10).

RR Structure. Although the active form of RR is typically depicted in the literature as an $R1_2R2_2$ heterodimer, our results demonstrate that the $R1_6R2_6$ heterohexamer has essentially the same activity per R1 monomer and, given the nucleotide substrate and effector concentrations present in vivo, is likely to be the major active form of the enzyme in mammalian cells. This conclusion is consistent with the

Scheme 2: Importance of the A-Site in the Aggregation of R1[a]

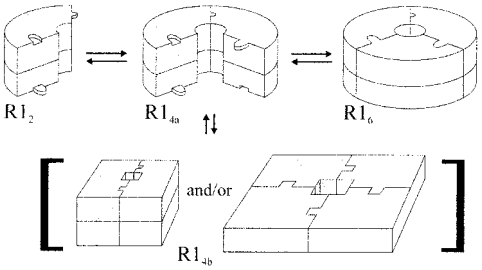

[a] The R1 dimer has two a-sites, shown as projections, and two a-site receptors, shown complementary to the a-site projection, but no a-site−receptor interactions. The R1 tetramer has an open form, having two such interactions, and two possible closed forms, each having four a-site−receptor interactions. The closed R1 hexamer has six such interactions. Tetramer isomerization could involve substantial structural change.

crystal structure of *Escherichia coli* R1 (eR1), the only determined R1 structure, which shows R1 to be a hexamer, i.e., a trimer of three identical dimers (*27*).

Because of the clear sequence homology between mR1 and eR1 (*28*), it is reasonable to use the eR1 hexamer structure in interpreting our results for mR1. The cartoon shown in Scheme 2 provides a possible structural rationale for Scheme 1. Here the projecting part of the structure corresponds to the N-terminal region making the dimer−dimer contact (Figure 12) which structural, genetic, and biochemical studies strongly implicate as the location of the a-site (*29*). Depicting $R1_2$ as shown in structure 1 leads to speculation that $R1_2$ dimerization first leads to an "open" form of $R1_4$, in which only two of four potential dimer−dimer contacts are made. This open form can either isomerize to a "closed" form or forms, in which all four contacts are made, or react with a third $R1_2$, forming closed $R1_6$ in which there are six dimer−dimer contacts. From the parameter values given in Table 4, $R1_{4b}$ is more stable than $R1_6$ in the absence of ATP binding to the h-site. It is tempting to speculate that the open and closed forms of $R1_4$ correspond in Scheme 1 to $R1_{4a}$ and $R1_{4b}$, respectively, with the increase in the number of dimer−dimer subunit contacts accounting for K_{is} values of $\gg 1$ and the conformational change implicit in conversion of open to closed forms providing a rationale for the slowness of the process. It may also be that full stabilization of the $R1_{4b}$ closed form requires ATP or dATP binding to the a-site, and the high activity retained in dGTP- or dTTP-induced tetramers is due to a lack of conversion of a more active $R1_{4a}$ form to a less active $R1_{4b}$ form.

Why does tetramer formation result in low enzymatic activity? We at first speculated that the low specific activity of $R1_{4b}$ (and possibly of $R1_{4a}$) might be due to an inability to form a complex with $R2_2$. However, this is not the case, since increasing the $R2_2$ concentration (3-fold, data not shown) had no effect on the dATP concentration required for inhibition of dTTP-dependent GDP reductase (Figure 8). If the R1 tetramer were unable to bind $R2_2$, increasing the $R2_2$ concentration would favor $R1_2$ over $R1_4$, with the result being that higher dATP concentrations would have been required for inhibition of enzymatic activity. It remains possible that $R2_2$ binding to $R1_{4b}$ (and possibly to $R1_{4a}$ as well) is distorted vis-à-vis $R2_2$ binding to either $R1_2$ or $R1_6$, and that such distortion results in a slower rate of electron transfer between the Y177 free radical in mR2 (Y122 in eR2) and the active site in mR1. Such rates are exquisitely sensitive to distance and pathway (*30*−*32*).

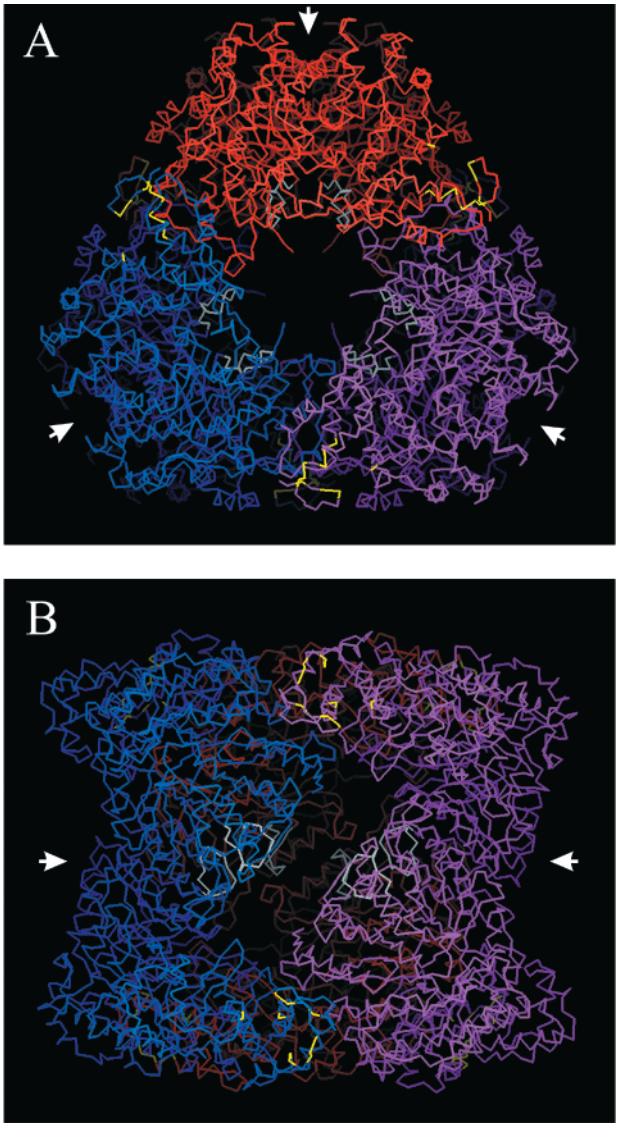

FIGURE 12: Structure of $R1_6$ from *E. coli* (PDB entry 1RLR) with both the AMP-PNP and the proposed $R2_2$ binding sites highlighted, C_α trace (*23*, *24*): (red, purple, or blue) R1 dimers within the R1 hexamer, (yellow) residues which contact the ATP analogue AMP-PNP, and (gray) R1 residues within 13 Å of R2 residue Phe47, which is at the $R1_2$−$R2_2$ interface in the docked model. Views are with the 3-fold rotational symmetry axis (A) perpendicular or (B) parallel to the plane of the page. The large white arrows indicate a possible docking site for $R2_2$ binding to $R1_2$ that is accessible in $R1_6$.

Finally, the similarity of dissociation constants for $R2_2$ binding either $R1_2$ (*15*) or $R1_6$ (this work) implies that the $R2_2$ binding site(s) should be similar on both $R1_2$ and $R1_6$. This assumption excludes $R2_2$ from binding $R1_2$ as indicated in an earlier docked model of the $R1_2R2_2$ complex (*33*), since, in this model (Figure 12), R1 residues contacting R2 lie at the interior of the $R1_6$ hexamer structure, a physical impossibility. This conclusion has obvious consequences for previous studies (*34*, *35*) that have used the docked $R1_2R2_2$ complex structure to rationalize losses of enzyme activity resulting from mutations in R1, on the basis of perturbation of radical transfer between the two subunits of the enzyme.

It emphasizes the need, in the absence of a crystal structure of the holoenzyme, for a new computational subunit docking study using $R1_6$, rather than $R1_2$, as the docking surface.

In conclusion, while Scheme 1 provides a satisfactory explanation for many aspects of the allosteric regulation of RR enzymatic activity, it leaves several important questions unresolved, including (a) the enzymatic activity of the $R2_2$ complex of $R1_{4a}$, (b) the location of the putative h-site, (c) the structure of the holoenzyme, (d) the energetics of hexamer formation, and (e) the nature of structural differences between $R1_{4b}$ and $R1_6$. Experiments are underway in this laboratory to address these questions.

ACKNOWLEDGMENT

We gratefully acknowledge Nora Zuño for her excellent technical assistance, Ronen Marmorstein and Adrienne Clements for their help in taking DLS measurements, and Ulla Uhlin for providing the coordinates of the docked model of eR2 bound to eR1.

SUPPORTING INFORMATION AVAILABLE

Curve fitting and sedimentation studies on R1. This material is available free of charge via the Internet at http://pubs.acs.org.

REFERENCES

1. Jordan, A., and Reichard, P. (1998) *Annu. Rev. Biochem. 67*, 71−98.
2. Stubbe, J., and van der Donk, W. A. (1995) *Chem. Biol. 2*, 793−801.
3. Thelander, L., and Reichard, P. (1979) *Annu. Rev. Biochem. 48*, 133−158.
4. Reichard, P., Eliasson, R., Ingemarson, R., and Thelander, L. (2000) *J. Biol. Chem. 275*, 33021−33026.
5. Brown, N. C., and Reichard, P. (1969) *J. Mol. Biol. 46*, 39−55.
6. Thelander, L., Eriksson, S., and Åkerman, M. (1980) *J. Biol. Chem. 255*, 7426−7432.
7. Larsson, A., and Reichard, P. (1966) *J. Biol. Chem. 241*, 2533−2539.
8. Larsson, A., and Reichard, P. (1966) *J. Biol. Chem. 241*, 2540−2549.
9. Eriksson, S., Thelander, L., and Åkerman, M. (1979) *Biochemistry 18*, 2948−2952.
10. Chang, C. H., and Cheng, Y. C. (1979) *Cancer Res. 39*, 5087−5092.
11. Brown, N. C., and Reichard, P. (1969) *J. Mol. Biol. 46*, 25−38.
12. Thelander, L. (1973) *J. Biol. Chem. 248*, 4591−4601.
13. Cory, J. G., and Fleischer, A. E. (1982) *Arch. Biochem. Biophys. 217*, 546−551.
14. Chimploy, K., and Mathews, C. K. (2001) *J. Biol. Chem. 276*, 7093−7100.
15. Scott, C. P., Kashlan, O. B., Lear, J. D., and Cooperman, B. S. (2001) *Biochemistry 40*, 1651−1661.
16. Wyatt, P. J. (1993) *Anal. Chim. Acta 272*, 1−40.
17. Cantor, C. R., and Schimmel, P. R. (1980) *Biophysical Chemistry*, Freeman and Company, New York.
18. Ingemarson, R., and Thelander, L. (1996) *Biochemistry 35*, 8603−8609.
19. Erickson, H. K. (2000) *Biochemistry 39*, 9241−9250.
20. Eriksson, S. (1983) *J. Biol. Chem. 258*, 5674−5678.
21. Traut, T. W. (1994) *Mol. Cell. Biochem. 140*, 1−22.
22. Kennedy, H. J., Pouli, A. E., Ainscow, E. K., Jouaville, L. S., Rizzuto, R., and Rutter, G. A. (1999) *J. Biol. Chem. 274*, 13281−13291.
23. International Human Genome Sequencing Consortium (2001) *Nature 409*, 860−921.
24. Hendricks, S. P., and Mathews, C. K. (1997) *J. Biol. Chem. 272*, 2861−2865.
25. Cory, J. G., and Fleischer, A. E. (1979) *Cancer Res. 39*, 4600−4604.
26. Jackson, R. C. (1984) *Pharmacol. Ther. 24*, 279−301.
27. Uhlin, U., Uhlin, T., and Eklund, H. (1993) *FEBS Lett. 336*, 148−152.
28. Pender, B. A., Wu, X., Axelsen, P. H., and Cooperman, B. S. (2001) *J. Med. Chem. 44*, 36−46.
29. Eriksson, M., Uhlin, U., Ramaswamy, S., Ekberg, M., Regnstrom, K., Sjöberg, B. M., and Eklund, H. (1997) *Structure 5*, 1077−1092.
30. Beratan, D. N., Onuchic, J. N., Winkler, J. R., and Gray, H. B. (1992) *Science 258*, 1740−1741.
31. Moser, C. C., Keske, J. M., Warncke, K., Farid, R. S., and Dutton, P. L. (1992) *Nature 355*, 796−802.
32. Rova, U., Goodtzova, K., Ingemarson, R., Behravan, G., Gräslund, A., and Thelander, L. (1995) *Biochemistry 34*, 4267−4275.
33. Uhlin, U., and Eklund, H. (1994) *Nature 370*, 533−539.
34. Ekberg, M., Sahlin, M., Eriksson, M., and Sjoberg, B. M. (1996) *J. Biol. Chem. 271*, 20655−20659.
35. Ekberg, M., Potsch, S., Sandin, E., Thunnissen, M., Nordlund, P., Sahlin, M., and Sjoberg, B. M. (1998) *J. Biol. Chem. 273*, 21003−21008.
36. de Korte, D., Haverkort, W. A., van Gennip, A. H., and Roos, D. (1985) *Anal. Biochem. 147*, 197−209.
37. Jackson, R. C., Lui, M. S., Boritzki, T. J., Morris, H. P., and Weber, G. (1980) *Cancer Res. 40*, 1286−1291.
38. Kemp, A. J., Lyons, S. D., and Christopherson, R. I. (1986) *J. Biol. Chem. 261*, 14891−14895.

BI011653A